Basic Medical Research

Multi-hole spherical CT scan method to characterize large quantities of bones in rats

Neng Nenden Mulyaningsih,[1,2] Ariadne Lakshmidevi Juwono,[1] Djarwani Soeharso Soejoko,[1] Dewi Apri Astuti[3]

pISSN: 0853-1773 • eISSN: 2252-8083
https://doi.org/10.13181/mji.oa.215452
Med J Indones. 2021;30:182–90

Received: April 15, 2021
Accepted: July 20, 2021

Authors' affiliations:
[1]Department of Physics, Faculty of Mathematics and Natural Sciences, Universitas Indonesia, Depok, Indonesia, [2]Department of Physics Education, Faculty of Mathematics and Natural Sciences, Universitas Indraprasta PGRI, Jakarta, Indonesia, [3]Department of Nutrition and Feed Technology, Faculty of Animal Sciences, Institut Pertanian Bogor, Bogor, Indonesia

Corresponding author:
Neng Nenden Mulyaningsih
Department of Physics, Faculty of Mathematics and Natural Sciences, Universitas Indonesia, F Building, Pondok Cina, Beji, Depok 16424, West Java, Indonesia
Tel/Fax: +62-21-787-2610/ +62-21-786-3441
E-mail: neng.nenden51@ui.ac.id

ABSTRACT

BACKGROUND New therapeutic options are often explored in *in vivo* studies using animals like rats. Since rats are small, it is difficult to examine them in a computed tomography (CT) scan. This study aimed to introduce a multi-hole spherical model CT scan method as a new, fast, economical, and reliable method to characterize large quantities of rat bones at once in estimating the timing of osteoporosis in ovariectomized white rats.

METHODS 50 female white rats (12 weeks old) were treated as the control group, and 40 rats of the same age were ovariectomized to establish the osteoporosis model. Sham rats were sacrificed at 13, 15, 17, 19, and 21 weeks old, while the ovariectomized rats were sacrificed at 15, 17, 19, and 21 weeks old. Afterward, tibia bones were removed, placed in the multi-hole spherical model, and characterized using a CT scan. Their characteristics were compared using a scanning electron microscope (SEM), transmission electron microscopy (TEM), and X-ray diffraction (XRD).

RESULTS The Hounsfield unit scores resulted from the multi-hole spherical model CT scan method of tibia bones of rats were consistent with the percentage of the osteocyte cavities, canalicular diameters, and crystal size. The multi-hole spherical model CT scan method could produce 50 times more data than the SEM, TEM, or XRD.

CONCLUSIONS Multi-hole spherical model CT scan was considered good and reliable in assessing bone quality parameters in rat samples simultaneously.

KEYWORDS bone quality, CT scan, multi-hole spherical model, osteoporosis, ovariectomy

Dual-energy X-ray absorptiometry is the gold standard for measuring a bone mineral density, but it does not provide information on bone quality nor any insight into the architectural structure of bones. Bone microstructure, particularly trabecula, is important for determining bone strength.[1] Hence, a new method to evaluate this bone microstructure is important to solve these limitations.

Animal models of rats are commonly used in research because of their similar genetic, biological, and behavioral characteristics to humans. In addition, rats also reproduce very quickly and can adapt well to new environments. The price is also relatively low, and it can be purchased in large quantities.[2,3] Moreover, rats tend to be gentle and docile, making them easy to control. According to the National Human Genome Research Institute, most rats used in medical experiments were inbred and nearly genetically identical. This, in turn, makes the results of the experiment more uniform.[4]

Due to their relatively small size, rats are technically difficult to be analyzed using a computed tomography (CT) scan. Several methods that have been commonly used were atomic absorption spectrophotometer, ultraviolet-visible spectroscopy, Fourier transform infrared spectroscopy, Raman spectroscopy, X-ray diffraction (XRD), scanning electron microscope (SEM), and transmission electron microscope (TEM).[5,6] Those methods still have limitations because the sample testing was carried out one by one, resulting in a higher cost and relatively longer duration. Thus, this study was aimed to propose a multi-hole spherical model CT scan as a new, fast, economical, and reliable method to analyze rat bones.

METHODS

Study design and sample collection

This research was an experimental study using ovariectomized white rats model (*Rattus norvegicus*). The animal procedure protocols were approved by the Ethics Committee of the Faculty of Medicine, Universitas Indonesia (No: 500/UN2.F1/ETIK/2017). All actions taken on animal models followed the principles of the Declaration of Helsinki. Rats were maintained in the Department of Nutrient Science and Feed Technology, Faculty of Animal Husbandry, Institut Pertanian Bogor, and the ovariectomy process was carried out in the Laboratory of Experimental Surgery, Division of Surgery and Radiology, Department of Clinic, Reproduction and Pathology, Faculty of Veterinary Medicine, Institut Pertanian Bogor from January to December 2018.

Ninety rats (12 weeks old) were used and maintained in individual cages. Forty rats were ovariectomized, and 50 rats were used as the control group. At 13 weeks old, 10 rats of the control group were directly sacrificed. All medical measures (anesthesia, blood draw, and tissue/organ collection) were conducted by the veterinarian. Euthanasia was done using ketamine (40–80 mg/kg) and xylazine (5 mg/kg) intraperitoneal. Euthanasia was done every 2 weeks in the ovariectomized rats and control groups at 15, 17, 19 and 21 weeks old for each group. Thus, nine treatment groups were analyzed, namely the control group at 13, 15, 17, 19, and 21 weeks old, and the ovariectomized group at 15, 17, 19, and 21 weeks old. This study used 10 rats in each group. After being sacrificed, the tibia bone was collected, cleaned from the attached muscles and soaked with hydrazine for 7 days, then rinsed and dried. Tibia bones were analyzed by a CT scan, SEM, TEM, and XRD.

Multi-hole spherical CT scan procedure

Multi-hole spherical was made using a wax-based material that resembled a human head (sphere) model with a diameter of 16 cm. It consisted of two parts, the upper half and lower half of the spherical model, which had 50 holes in total. Each hole had a depth of 3 cm and a diameter of 0.6 cm, as shown in Figure 1. Each hole was filled with one tibia bone. A gap in the hole was then filled with the remaining material to minimize the presence of air. All multi-hole spherical model manufacturing activities were carried out in the Mechanic Workshop Laboratory of the Department of Physics, Universitas Indonesia, Depok, Indonesia. The multi-hole spherical model with bone samples was merged to the upper and lower parts and characterized using a CT scan (General Electric BrightSpeed 16 Healthcare, UK). When the upper and lower were merged, different bones would be read as one. The following scan parameters were used: 16 mm × 0.625 mm collimation mode, rotational time of 0.8 sec, coverage of 500 mm, pitch of 1.75:1 at 260 mA, speed of 22 mm/s, and scan time of 24 sec. In this study, a 64-slice CT scan was used, but images representing the tibia bone were taken 12 slices because the 26 upper slices and 26 lower slices hit the multi-hole spherical model material instead of the tibia bone. The CT scan data analyzed were in the

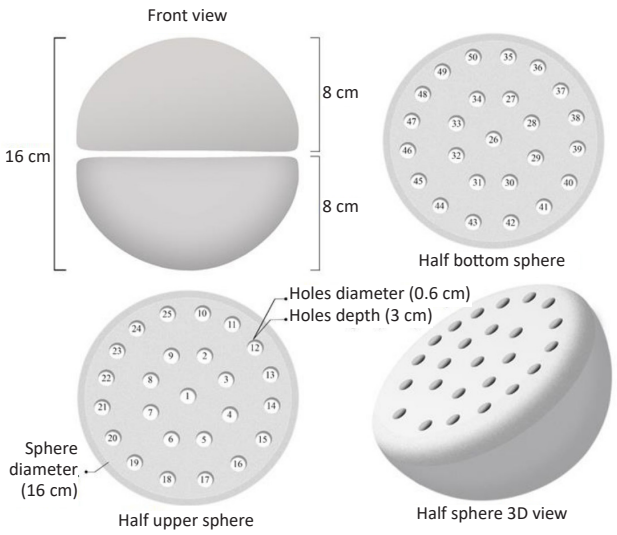

Figure 1. Multi-hole spherical model for bone density measurement with a computed tomography (CT) scan

form of the Hounsfield unit (HU) value. HU score as a bone density parameter consisted of 12 scores from 12 slices. The CT scan was conducted in the Department of Radiology, Cipto Mangunkusumo Hospital, Jakarta, Indonesia.

Scanning electron microscope (SEM) and transmission electron microscopy (TEM) procedure

To ensure that the method was done accordingly, the measurements were also carried out using the Hitachi S-3400N SEM (Hitachi High-Tech America, Inc., USA) in the Center for Materials and Processing Failure Analysis, Faculty of Engineering and the Tecnai 200 kV D2360 TEM Super Twin (Thermo Fisher Scientific, USA) in the Integrated Laboratory and Research Center, Universitas Indonesia. The upper end (proximal) of the tibial cortical region was characterized by an SEM. The resulting SEM image was then analyzed using the ImageJ application version 1.46r (National Institutes of Health, USA). Canalicular diameters and the percentage of the osteocyte cavities were also evaluated.

For the TEM analysis, thin sections of trabecular bone were cut using an ultra-cut microtome with an ultra-diamond knife and mounted on single-slot Formvar-coated grids. TEM images were taken at 19,500× magnification. Crystal-collagen interactions at the nanostructural level were analyzed from the TEM images for the shape, orientation direction, and alignment of apatite crystals in collagen fibril.

X-ray diffraction (XRD) procedure

The parameters analyzed using the XRD were the crystal size of the tibia using the Debye Scherrer equation. The tibia bone was crushed into powder with mortar, then 5 g of each sample was taken and placed in the sample holder until it was full and ready to be characterized. The XRD machine used was Rigaku MiniFlex 600 diffractometer (Rigaku MiniFlex, Japan) with Cu target metal, which had a wavelength of K-α1 = 1.54060 Å, K-α2 = 1.54443 Å, and K-β = 1.39225 Å. This tool was operated at 25°C with a voltage of 40 kV and a strong current of 30 mA. The 2θ diffraction angle started at 20° and ended at 80°, with a step size of 0.013° and a scan step time of 8.670 sec. The output of the XRD machine was presented as a diffractogram, which showed the relationship between the diffraction angle (2θ) and the intensity of the reflected X-rays. The output data from the XRD machine in raw data were identified and processed using the HighScore Plus program (Malvern Panalytical, UK) by Rietveld analysis to refine the crystal structure. This study was conducted in NanoTech Puspitek Serpong, Tangerang, Indonesia.

Experimental design

The calculation time was grouped into two categories: inactive time and active time. The duration of all periods was manually recorded. Inactive time was calculated from the preparation to become a multi-hole spherical model. The scanner was considered active when the multi-hole spherical model was inserted. Active time was divided into two categories: diagnostic studies and CT data analysis. Diagnostic study time was further divided into three categories: preparation, scanning, and take-down time. Preparation time was the time from the preparation, positioning, and placement of the multi-hole spherical model to the actual scan time. Scan time included the interval time between the contrast injection time, after contrast injection to the result time, and reviewing image time and the confirmation of completion by a radiologist. Take-down time was the time interval between the access removal and removal of the multi-hole spherical model from the scanner bed. Total examination or procedure time was defined as the multi-hole spherical model from the beginning to the end of the inspection time.

Image analysis

The CT scan technique was performed using the helical multiple slice sequence technique. All CT image data were imported to a personal computer workstation. The identification of the tibia was performed in each animal model under a constant window (window width 1100; window level 100). At each cross-section, the density of the four cortical bone (anterior, posterior, medial, and lateral) and region of interest (ROI) (diameter 3 mm and area of 15,169 ± 253.838) were measured. To evaluate the variations of observations, the ROI values measurement was repeated 10 times. The elliptical selections of the ROI, which consisted exclusively of the cortical bones of the rat's tibia, were drawn and seen using the ImageJ software. For each ROI, the mean HU values were calculated and recorded. The average of the four cortical values was calculated and described as cortical bone density.

Statistical analysis

The mean, standard deviation, and confidence interval were measured for all sample groups. The paired *t*-test was used to analyze the HU scores and canalicular diameter of cortical and trabecular bone. The *t*-test analysis was used to compare each parameter between the control and treatment groups and between the treatment groups. In addition, the *t*-test analysis was also used to compare the HU values at the ends with the middle of the bones in the same group. As an alternative to the *t*-test, the Wilcoxon test was used. All data were analyzed using SPSS software version 22.0 (IBM Corp., USA). The value of $p<0.05$ was considered statistically significant.

RESULTS

The duration of scanning 50 tibia bones using a multi-hole spherical model at once was relatively short. This stage was only conducted once, which took about 16 hours (2 full working days). Then, the multi-hole spherical model can be used repeatedly. The diagnostic study time, which included preparation time, approximately took 30 min. Setting the irradiation field and the irradiation process approximately took 15 min, and the take-down time was about 10 min. The diagnostic study only took 55 min to obtain data from 50 samples directly. Meanwhile, data analyzing time highly depended on the expertise of the data reader or researcher because the output data from the CT scan were directly transferred to the computer system.

Multi-hole spherical model trial test

Based on the HU values, using a multi-hole spherical model in analyzing rat bones using a CT scan can detect osteoporotic changes in the tibia bone due to ovariectomy. The condition of osteoporosis and osteopenia is seen from the CT scan image of slices 1, 2, 11, and 12, as shown in Figure 2. Slices 1 and 2 were the two end slices in the distal part of the tibia, while slices 11 and 12 were the two most end slices in the proximal part of the tibia. Of the four slices, the control group showed a full white area. In the 15 weeks old ovariectomized rat group, black color in the middle part started to appear. Similarly, the 17 and 21 weeks old ovariectomized rat groups showed a bigger black color in the middle parts. The widening of the black color in the middle decreased the HU value.

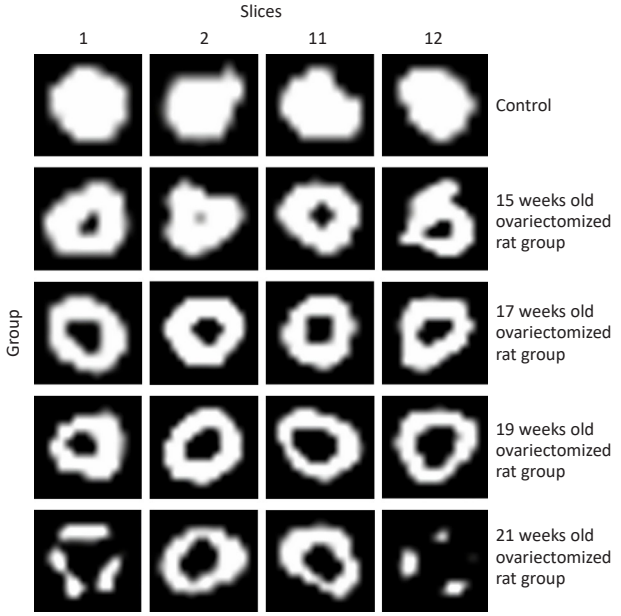

Figure 2. The computed tomography (CT) scan images of slice at the distal (no. 1 and 2) and proximal (no. 11 and 12) of the tibia (15× magnification)

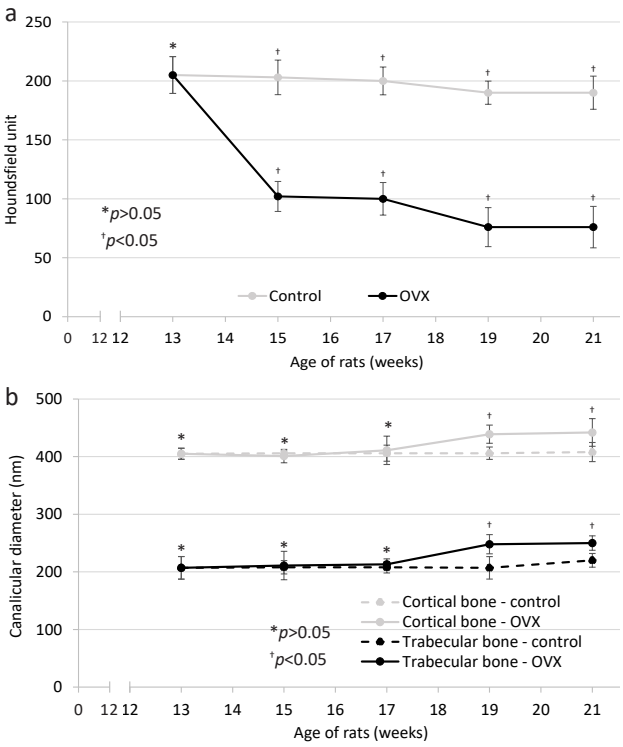

Figure 3. The tibia in rats developing osteoporosis based on age. (a) HU on the tibia slice 12 (proximal tibia); (b) canalicular diameters. The value of $p<0.05$ was considered statistically significant. HU=Hounsfield unit; OVX=ovariectomized

Based on the results, more extreme changes occurred at the end of the bones (proximal and distal). The HU score of the upper/proximal bone (slice 12) is shown in Figure 3a. Rats aged 13 weeks old (control

group) had HU scores of 205 ± 16, and it decreased by 50.2% to 102 ± 13 in the 15 weeks old ovariectomized rat group. Furthermore, it decreased by 51.2%, 62.9%, and 62.9%, respectively, compared with the 17, 19, and 21 weeks old rats in the control group. Based on the HU score, the tibia bone in the 15 and 17 weeks ovariectomized rat groups showed osteopenia in the 3rd and 5th weeks after ovariectomy. Meanwhile, osteoporosis began to appear in the 7th week after ovariectomy (19 weeks old ovariectomized rat group) and constantly appeared until the 9th week (21 weeks old ovariectomized rat group).

Bone morphology analysis

The CT scan results were supported by the SEM and TEM imaging analysis results, as shown in Figure 4a. The SEM image showed that the longer the time after ovariectomy, the greater the degree of damage seen in the tibial cavity, with the deeper cavities appeared darker on the SEM images. The SEM characterization results for the tibia in the control group (Figure 4a[i]) appeared to have a smooth surface with fewer cavities. The cavities in Figure 4a(ii) (15 weeks old ovariectomized rat group) show a relatively small size cavities enlargement. Figure 4a(iii) (17 weeks old ovariectomized rat group) shows many cavities and rough fibers. Figure 4a(iv) (19 weeks old ovariectomized rat group) shows a surface that has larger fibers and is likely to peel off. Figure 4a(v) (21 weeks old ovariectomized rat group) shows clearer and deeper cavities.

The SEM images of the tibia bone in the control and ovariectomized groups were also analyzed using ImageJ. The average osteocyte cavities and canalicular diameters was obtained. The average score of the osteocyte cavities intensity in the 15 to

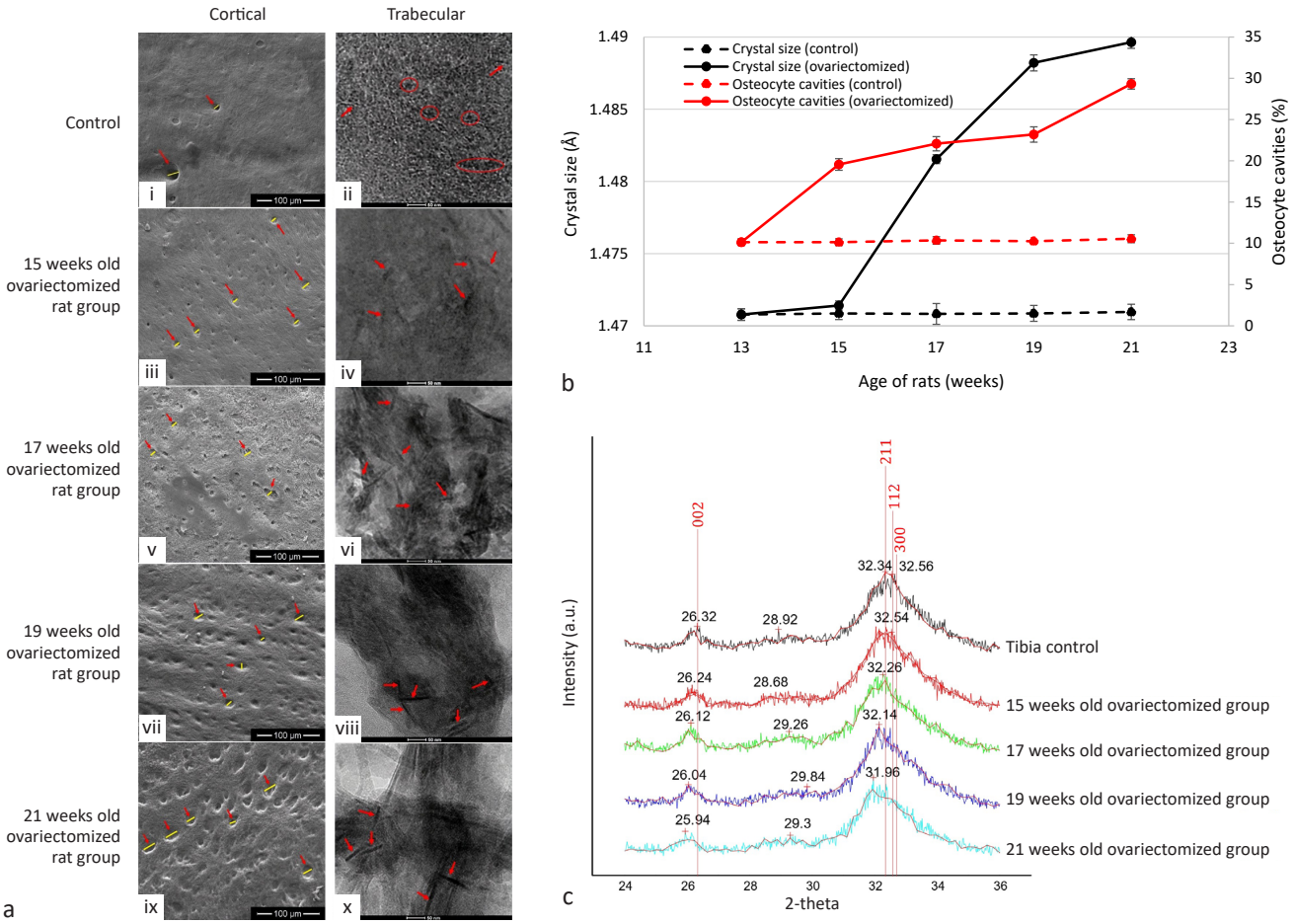

Figure 4. (a) SEM and TEM images of the tibia bone. (i, iii, v, vii, ix) SEM of the cortical bone, red arrows=osteocyte cavities, yellow lines=canalicular diameters. (ii, iv, vi, viii, x) TEM images of the trabecular bone, red arrows=needle-like elongated crystals, red circles=plate like crystals; (b) average of crystal size (Å) and the percentage of osteocyte cavities; (c) XRD spectra from the tibia bone control and time after ovariectomy. SEM=scanning electron microscope; TEM=transmission electron microscope; XRD=X-ray diffraction

21 weeks old ovariectomized rat groups showed an increasing pattern. Three to 7 weeks after ovariectomy, the percentage of the cavities intensity increased twice, compared with the normal tibia bone cavities. Nine weeks since ovariectomy, the percentage of the cavities intensity had tripled the normal (21 weeks old control rats) tibia bone cavities. Thus, the highest level of bone damage occurred in the 21 weeks old ovariectomized rat group. Five weeks after ovariectomy, the canalicular diameter was 411 ± 25 nm *versus* 406 ± 14 nm in the control group at the same age (p = 0.292). Seven weeks after ovariectomy, the canalicular diameter increased compared with the control at the same age (439 ± 16 nm *versus* 406 ± 11 nm, $p = 1.710 \times r^{-5}$). It also increased in 9 weeks after ovariectomy (442 ± 24 nm), compared with the control at the same age (408 ± 17 nm) with p = 0.001. The cortical bone SEM images showed significantly different osteocyte cavities (red arrows) and canalicular diameters (yellow lines) between the 19 and 21 weeks old ovariectomized rat groups (Figure 4, a[iv] and a[v]).

TEM images of the tibia in the trabecular region showed nanoscale structures, as shown in Figure 4a[vi–x]. In the control group (Figure 4a[vi]), the crystals appeared to have two dominant shapes, namely a plate-like shape (red circle) and elongated needle-like shape (red arrow). In contrast, each image of the ovariectomized rat group as a whole (Figure 4a[vii–x]) had a needle-like crystal shape. In the control group, the crystal structures were scattered randomly and tightly in small sizes. In certain regions, some patterns appeared in a circular orientation. The crystal structures in the ovariectomized group were almost the same as the control, but it was more random and irregular. Likewise, the canalicular diameter also appeared larger. The regular canalicular diameter of trabecular bone in the tibia control group was 207 ± 20 nm and increased up to 248 ± 17 nm in the 19 weeks old ovariectomized rat group with $p = 4.160 \times r^{-5}$ and still relatively constant in the 21 weeks old ovariectomized rat group (250 ± 13 nm) *versus* 220 ± 12 nm in the control group ($p = 1.650 \times r^{-5}$), as shown in Figure 3b. The SEM and TEM analyses showed that the ovariectomized group had a greater effective canalicular diameter. The canalicular diameter started to show significantly different values in the 19 weeks old ovariectomized rat group and was relatively constant until 21 weeks old.

The increase in osteocyte cavities percentage was comparable with the increase in crystal size, as shown in Figure 4b. The 21 weeks old ovariectomized rat group had the crystal size, and the osteocyte cavities increased by 1.34% and 65.42%, respectively, compared with the control group. Other comparative data were the result of characterization with XRD, as shown in Figure 4c. The XRD data records were analyzed at a 2-theta angle between 24°–36°. There were two dominant peaks with relatively high intensity, namely at 2-theta between 25°–27° and 31°–34°. A 2-theta between 25°–27° showed a 2-theta angle shifted to the left of the ovariectomized rat group. This angle was in the reflection factor (002) plane, while the 2-theta angle between 31°–34° showed overlapping peaks in the reflection factors (211), (112), and (300), making it wider and difficult to analyze.

DISCUSSION

In this study, the result of a multi-hole spherical model CT scan to analyze many rat bones at once was consistent. This study lays the groundwork for further pre-experiment studies and shows the potential of a multi-hole spherical model CT scan in the translational process of quantitative imaging analysis for routine experimental practice. In the last decades, CT applications have acquired a fundamental role in diagnostic imaging, resulting in an increasing demand for visual examination by radiologists.[7] In the biomaterial science research community, visual sample or morphological analysis can be performed using an SEM or TEM.[8,9] However, these two tools have limitations in the sample preparation used.[10] Sampling using organisms should be characterized using an SEM or TEM and must be taken and separated from the organisms, which requires surgery.[11] Meanwhile, characterization using a CT scan can be done without separating the parts of the body. One of the methods used is the morphological analysis of a material, with bone density as the most commonly used material. In analyzing bone density using a CT scan, the femur, tibia, or spine of the bone can be directly prepared without any special pre-treatment. In contrast, the SEM or TEM requires special pre-treatment, such as grinding the bones. For conventional imaging using SEM, the specimen must be electrically conductive. Thus, the bone must be firstly coated with an ultra-thin layer of electrically conductive material, such

as gold or platinum, deposited on the sample. This metallic coating can increase the signal or noise ratio of the sample. In addition, TEM is a fairly complicated procedure because the samples used must be very thin, and the preparation technique should not induce any artifacts, such as precipitates or amorphization. Therefore, CT scan is the best technique for bone characterization based on its convenient sample preparation.

Research using animal models is continually used until today. However, specific investigation on rat bones using a CT scan is rarely used. The main advantage of this methodological approach is using the same scanner for different bones with the same protocol, thus eliminating confounders observed in most clinical studies, such as longer duration between the scans, repositioning, or anatomical changes of the target volume. In addition, intra- and interscanner differences resulting from the CT vendor-specific characteristics, as well as different technological developments or local institutional preferences and post-processing of acquired images, result in a lack of standardization.[12,13]

Apart from the clinical approaches, most conventional CT phantoms for the comprehensive scanning evaluation are not applicable for quantitative feature analyses due to their lack of a textural background.[14] Therefore, we designed a customized multi-hole spherical model, which is a feasible tool for investigating the repeatability and reproducibility of bone parameters in general. Additionally, the materials used are close to human tissue, thus closing the gap between the non-human model and preclinical study designs.[15]

This study found that CT scan images are more informative in representing the osteoporosis process resulting from ovariectomy (Figure 2) compared with the SEM or TEM images (Figure 4a). This observation is an important basis of recommendation in selecting the characterization tools used to analyze bones, especially rat bones.

Previous researchers have analyzed a bone density based on the HU scores of a CT scan.[16] The CT scan has been commonly used to diagnose bone and soft tissue. However, the scanned objects are still limited to relatively large samples (human scale). Therefore, special methods are needed to characterize relatively small samples such as rat bones with a CT scan. Using intermediary media such as multi-hole spherical model may overcome the problem. A multi-hole spherical model is a specially designed object scanned or imaged in the medical imaging field to evaluate, analyze, and adjust the performance of various imaging devices. This model can characterize small-sized samples and allows direct application to humans (large-sized samples compared with rats). In small-sized samples (rat bone), it can characterize large amounts of sample data simultaneously. In addition, the speed in producing data is relatively fast. In the diagnostic study, it takes a total of approximately 55 min from the preparation to the data generation. The data are produced in one direct process from 50 data objects, thus required 1.1 min on average for each sample.

CT scan showed the process of osteoporosis. It was supported by the crystal size data obtained from the XRD spectra trailer at 2-theta between 24° until 36°, representing the diffraction angle as shown in Figure 4c. Based on the figure, there were two dominant peaks with relatively high intensity, namely at 2-theta between 25°–27° that corresponded to the field position (002), and 2-theta between 31°–34° that seemed overlapping with field (211), (112), and (300), making it more difficult to analyze. In the field shift (002), there was a shift in the 2-theta angle to the left in the ovariectomized rat group. The 2-theta values in the control and 21 weeks old ovariectomized rat groups were 26.32° and 25.94°, respectively. Based on the Scherrer equation, a decrease in the 2-theta angle value in ovariectomized rats would cause a longer and thinner crystal size.

On the XRD, there was only a peak of hydroxyapatite crystal and no other crystal phases. The diffraction pattern showed that crystal size was larger and significantly different with $p<0.05$, compare with the 19 weeks old ovariectomized rat group (Figure 4b). Thus, the osteoporosis characteristics started to appear at the 7th week after ovariectomy. A large crystal size indicates a higher porosity.[17,18]

The multi-hole spherical model CT scan protocols were applied to close the intact bone and visually investigated in the cross-sectional sections. Based on the HU score, the tibia bone density measurement result was consistent with the SEM, TEM, and XRD results. Based on the CT scan, the middle tibia bone had a higher HU score because the central part was composed of denser cortical bone, resulting in a higher density. In contrast, both the upper end (proximal) and the lower end (distal) of the bone

showed a lower HU score compare with the center. As it was composed of trabecular bone, the density was lower.[19,20]

In our study, the results of the SEM, TEM, and XRD analyses supported the analytical data obtained from the multi-hole spherical model CT scan. The new method might be a valuable medical diagnostic tool essential for elucidating diseases and their therapies. CT scan can be a solution for practicality. However, another tool should be added to complement the characterization.[21,22] Recommendations for future research include comparison with other tools to test the suitability of this method. In addition, the images generated from the multi-hole spherical model CT scan can be analyzed and compared with other images such as micro CT.

Using a multi-hole spherical model in analyzing rat bones using a CT scan has provided several advantages, including a simple proposed model regarding its physical structure. A multi-hole spherical model of 50 holes can be more practical and faster as it can generate 50 data directly in less than 1 hour, which also reduced the cost. This model can be a leading innovation for advancing and developing an accurate and innovative multi-hole spherical model to replace the conventional irradiation technique. Thus, it will result in more accurate and cost-effective experiments and help the researchers test several different protocols and parameters and gain valuable knowledge for the bone remodeling process. A standardized preparation procedure should be made to improve the use of the multi-hole spherical model.

However, using a multi-hole spherical model CT scan in analyzing rat bones still has some limitations. Improvements in preparing samples for CT scanning and matching the data sample with hole codes should be conducted. In addition, the irregular shape of the bone may cause space in the hole, thus covering the void in the hole is necessary. Placing tibia bone samples in the multi-hole spherical model should also be done carefully and thoroughly to avoid misreading the bone number. In this study, the images, either the CT scan, SEM, or TEM, were subjectively analyzed because it was based on the assumptions of the researchers or the operators. A high-contrast resolution test was conducted to reduce the subjectivity. A line pair image to determine the resolution was used and plotted using ImageJ software to produce more objective data.

Furthermore, the multi-hole spherical model had the same hole size despite different bone sizes and shapes. No rules on sample placement had been determined. Thus, the effect of object position on the measured noise value is still negligible. Considering the geometric aspects such as spatial position, object size, shape, and other specifications is suggested in using this multi-hole spherical model. Although it has some limitations, determining osteoporosis in ovariectomized white rats with the multi-hole spherical model CT scan can be considered one of the new methods to characterize small-sized samples (rat bones) simultaneously, resulting in more efficient and cost-effective experiments.

Conflict of Interest

The authors affirm no conflict of interest in this study.

Acknowledgment

The authors would like to acknowledge the Universitas Indonesia for the financial and technical support to carry out this research through "*Hibah* TADOK Universitas Indonesia".

Funding Sources

This study was funded by *Hibah* TADOK Universitas Indonesia with letter of decree No. 1331/UN2.R3.1/HKP.05.00/2018.

REFERENCES

1. Pennington Z, Ehresman J, Lubelski D, Cottrill E, Schilling A, Ahmed AK, et al. Assessing underlying bone quality in spine surgery patients: a narrative review of dual-energy X-ray absorptiometry (DXA) and alternatives. Spine J. 2021;21(2):321–31.
2. Manns M, Basbasse YE, Freund N, Ocklenburg S. Paw preferences in mice and rats: meta-analysis. Neurosci Biobehav Rev. 2021;127:593–606.
3. Zolocinska A, Siennicka K, Debski T, Gut G, Mazur S, Gajewska M, et al. Comparison of mouse, rat and rabbit models for adipose - Derived stem cells (ASC) research. Curr Res Transl Med. 2020;68(4):205–10.
4. Parker CC, Chen H, Flagel SB, Geurts AM, Richards JB, Robinson TE, et al. Rats are the smart choice: rationale for a renewed focus on rats in behavioral genetics. Neuropharmacology. 2014;76 Pt B(0 0):250–8.
5. Mitić Ž, Stolić A, Stojanović S, Najman S, Ignjatović N, Nikolić G, et al. Instrumental methods and techniques for structural and physicochemical characterization of biomaterials and bone tissue: a review. Mat Sci Eng C Mater Biol Appl. 2017;79:930–49.
6. Ramahwati MN, Juwono AL, Soejoko DS, Mulyaningsih NN. Analysis of morphology and absorption of calcium and magnesium for calcium phosphate Ca3(PO4)2 in rat's spine. IOP Conf Ser Mater Sci Eng. 2019;496:012039.
7. Doria S, Valeri F, Lasagni L, Sanguineti V, Ragonesi R, Akbar MU, et al. Addressing signal alterations induced in CT images by deep learning processing: a preliminary phantom study. Phys Med. 2021;83:88–100.
8. Hembrick-Hollomana V, Samuel T, Mohammeda Z, Jeelani S, Rangari VK. Ecofriendly production of bioactive tissue engineering scaffolds derived from egg- and sea-shells. J Mater Res Technol. 2020;9(6):13729–39.
9. Mulyaningsih NN, Juwono AL, Soejoko DS, Astuti DA. Morphology of proximal cortical epiphysis bone of ovariectomized Rattus

Norvegicus. Turk J Osteporos. 2020;26:169–74.
10. Okumura T, Shoji M, Hisada A, Ominami Y, Ito S, Ushiki T, et al. Electron tomography of whole cultured cells using novel transmission electron imaging technique. Micron. 2018;104:21–5.
11. Falsafi SR, Rostamabadi H, Assadpour E, Jafari SM. Morphology and microstructural analysis of bioactive-loaded micro/nanocarriers via microscopy techniques; CLSM/SEM/TEM/AFM. Adv Colloid Interface Sci. 2020;280:102166.
12. Ismail NA, Abdullah N, Mohamad Noor MH, Lai PS, Shafie MS, Nor FM. Accuracy and reliability of virtual femur measurement from CT scan. J Forensic Legal Med. 2019;63:11–7.
13. Carew RM, Viner MD, Conlogue G, Márquez-Grant N, Beckett S. Accuracy of computed radiography in osteometry: a comparison of digital imaging techniques and the effect of magnification. J Forensic Radiol Imaging. 2019;19:100348.
14. Yoshida Y, Yanagawa M, Hata A, Sato Y, Tsubamoto M, Doi S, et al. Quantitative volumetry of ground-glass nodules on high-spatial-resolution CT with 0.25-mm section thickness and 1024 matrix: phantom and clinical studies. Eur J Radiol Open. 2021;8:100362.
15. Racine D, Becce F, Viry A, Monnin P, Thomsen B, Verdun FR, et al. Task-based characterization of a deep learning image reconstruction and comparison with filtered back-projection and a partial model-based iterative reconstruction in abdominal CT: a phantom study. Phys Med. 2020;76:28–37.
16. Narayanan A, Cai A, Xi Y, Maalouf NM, Rubin C, Chhabra A. CT bone density analysis of low-impact proximal femur fractures using Hounsfield units. Clin Imaging. 2019;57:15–20.
17. Londoño-Restrepo SM, Herrera-Lara M, Bernal-Alvarez LR, Rivera-Muñoz EM, Rodriguez-García ME. In-situ XRD study of the crystal size transition of hydroxyapatite from swine bone. Ceram Int. 2020;46(15):24454–61.
18. Castillo-Paz AM, Londoño-Restrepo SM, Tirado-Mejía L, Mondragón MA, Rodríguez-García ME. Nano to micro size transition of hydroxyapatite in porcine bone during heat treatment with low heating rates. Prog Nat Sci Mater. 2020;30(4): 494–501.
19. McNerny EMB, Buening DT, Aref MW, Chen NX, Moe SM, Allen MR. Time course of rapid bone loss and cortical porosity formation observed by longitudinal μCT in a rat model of CKD. Bone. 2019;125:16–24.
20. Booz C, Noeske J, Albrecht MH, Lenga L, Martin SS, Yel I, et al. Diagnostic accuracy of quantitative dual-energy CT-based bone mineral density assessment in comparison to Hounsfield unit measurements using dual x-ray absorptiometry as standard of reference. European J Radiol. 2020;132:109321.
21. Shevroja E, Lamy O, Kohlmeier L, Koromani F, Rivadeneira F, Hans D. Use of trabecular bone score (TBS) as a complementary approach to dual-energy X-ray absorptiometry (DXA) for fracture risk assessment in clinical practice. J Clin Densitom. 2017;20(3):334–45.
22. Hunt HB, Donnelly E. Bone quality assessment techniques: geometric, compositional, and mechanical characterization from macroscale to nanoscale. Clinic Rev Bone Miner Metab. 2016;14(3):133–49.